Capturing Nonlinear Electron Dynamics with Fully Characterised Attosecond X-ray Pulses

Lars Funke[1*†], Markus Ilchen[2,4,5*†], Kristina Dingel[3],
Tommaso Mazza[4], Terence Mullins[4,5], Thorsten Otto[5],
Daniel Rivas[4], Sara Savio[1], Svitozar Serkez[4], Peter Walter[12],
Niclas Wieland[2], Lasse Wülfing[1], Sadia Bari[5,13], Rebecca Boll[4],
Markus Braune[5], Francesca Calegari[5], Alberto De Fanis[4],
Winfried Decking[5], Andreas Duensing[6], Stefan Düsterer[5],
Arno Ehresmann[3], Benjamin Erk[5],
Danilo Enoque Ferreira de Lima[4], Andreas Galler[4],
Gianluca Geloni[4], Jan Grünert[4], Marc Guetg[5], Patrik Grychtol[4],
Andreas Hans[3], Arne Held[1], Ruda Hindriksson[3], Ludger Inhester[5],
Till Jahnke[9], Joakim Laksman[4], Mats Larsson[7], Jia Liu[4],
Jon P. Marangos[8], Lutz Marder[3], David Meier[3], Michael Meyer[4],
Najmeh Mirian[5], Christian Ott[9], Christopher Passow[5],
Thomas Pfeifer[9], Patrick Rupprecht[9,10], Albert Schletter[6],
Philipp Schmidt[4], Frank Scholz[5], Simon Schott[4],
Evgeny Schneidmiller[5], Bernhard Sick[3], Sang-Kil Son[5],
Kai Tiedtke[5], Sergey Usenko[4], Vincent Wanie[5], Markus Wurzer[6],
Mikhail Yurkov[5], Vitali Zhaunerchyk[11], Wolfram Helml[1*]

[1]Fakultät Physik, Technische Universität Dortmund,
August-Schmidt-Straße 4, 44227 Dortmund, Germany.
[2]Institut für Experimentalphysik, Universität Hamburg, Luruper
Chaussee 149, 22761 Hamburg, Germany.
[3]Institut für Physik und CINSaT, Universität Kassel,
Heinrich-Plett-Straße 40, 34132 Kassel, Germany.
[4]European X-Ray Free-Electron Laser Facility GmbH, Holzkoppel 4,
22869 Schenefeld, Germany.
[5]Deutsches Elektronen-Synchrotron DESY, Notkestr. 85, 22607
Hamburg, Germany.
[6]Physik-Department, TUM School of Natural Sciences, Technische
Universität München, James-Franck-Straße 1, 85748 Garching, Germany.

[7]Department of Physics, AlbaNova University Center, Stockholm University, SE-106 91, Stockholm, Sweden.

[8]Blackett Laboratory, Imperial College London, London SW7 2AZ, United Kingdom.

[9]Max-Planck-Institut für Kernphysik, Saupfercheckweg 1, 69117 Heidelberg, Germany.

[10]Lawrence Berkeley National Laboratory, 1 Cyclotron Road, Berkeley, CA 94720 USA.

[11]Department of Physics, University of Gothenburg, 41296 Gothenburg, Sweden.

[12]SLAC National Accelerator Laboratory, 2575 Sand Hill Road, Menlo Park, CA 94025, USA.

[13]Zernike Institute for Advanced Materials, University of Groningen, 9747 AG Groningen, The Netherlands.

*Corresponding author(s). E-mail(s): lars.funke@tu-dortmund.de; markus.ilchen@uni-hamburg.de; wolfram.helml@tu-dortmund.de; [†]These authors contributed equally to this work.

Abstract

Attosecond X-ray pulses are the key to studying electron dynamics at their natural time scale involving specific electronic states. They are promising to build the conceptual bridge between physical and chemical photo-reaction processes. Free-electron lasers have demonstrated their capability of generating intense attosecond X-ray pulses. However, harnessing them for time-resolving experiments and investigations of nonlinear X-ray absorption mechanisms remains a cutting-edge challenge. We have characterised X-ray pulses with durations of down to 700 attoseconds and peak powers up to $200\,\mathrm{GW}$ at $\sim 1\,\mathrm{keV}$ photon energy via angular streaking at the SQS instrument of the European XFEL. As direct application, we present results of nonlinear X-ray–matter interaction via state-specific spectroscopy on a transient system. Using the derived spectral and temporal information of each pulse, we deliberately steer the probability for formation of double-core vacancies in neon gas atoms through excitation or ionisation of the second inner-shell electron after K-shell ionisation. Our results advance the field of attosecond science with highly intense and fully characterised X-ray pulses to the site-specific investigation of electronic motion in transient media.

1 Introduction

Attosecond physics based on high harmonic generation (HHG) of an optical laser has been developed from an experimental novelty to a Nobel prize-winning area of fundamental research [1, 2]. It has been extended to measurements of electron tunnelling in atoms [3], timing the photoemission from metal surfaces and bulk material [4] as well as to investigating their excited states in the form of plasmons [5]. Nevertheless, many desirable investigations have been hampered by the relatively low flux at higher photon energies achievable with HHG from longer driving laser wavelengths. Their limited energy tunability and challenging access to the X-ray regime [6, 7] are further constraints that can now be overcome by short-wavelength (X-ray) free-electron lasers (XFELs) [8].

Over the past decade, significant progress has been made in the compression of FEL pulses over the whole X-ray energy range [9, 10]. These advancements have been driven by various methodologies including non-linear compression [11], fresh slice techniques [12], emittance spoilers [13], and enhanced SASE methods [14]. Particularly noteworthy are the latest achievements in the vicinity of attosecond pulse durations within FELs, showcasing remarkable attosecond pump and probe capabilities [15, 16], as well as the generation of high peak power attosecond pulses [17]. The shortening of pulse durations from the femtosecond level to the attosecond scale represents a breakthrough in ultrafast FEL science due to their capability of producing highly intense X-ray pulses precisely tunable in photon energy, and thus to element-specifically address electrons in nonlinearly populated states [18].

These advancements offer efficient access to tracking energy-level rearrangement dynamics in atoms, molecules, and condensed matter, allowing the exploration of ultrafast processes in the dynamical origins of chemistry. Attosecond X-ray pulses create the opportunity for a direct observation of these charge redistribution dynamics in transient states such as electronic configuration changes in molecules [16, 19] and liquid water [20]. Moreover, the precise temporal characterization of single FEL pulses is an important prerequisite for the interpretation of experimental results from high-intensity coherent X-ray diffraction and imaging measurements [21, 22]. Entering the attosecond regime with full element specificity [14, 15, 23] and high pulse energies is, consequently, not merely an incremental step towards advanced time and spatial resolution, but rather the opening to a new scientific field with rich opportunities for understanding nature's dynamics literally at their core.

However, the underlying stochastic nature of the XFEL pulse generation by self-amplification of spontaneous emission (SASE) [24] limits the possible control of the X-ray pulses' time–energy structure. Despite several attempts to predict pulse characteristics using standard accelerator and photon diagnostics alongside machine learning (ML) approaches [25–27], accurate delivery of the time and energy structure especially with highly manipulated bunches for the production of attosecond pulses remains elusive. High-repetition-rate SASE XFELs [28] can mitigate this limitation by covering a broad pulse structure distribution, combined with a non-invasive pulse-by-pulse diagnostics and near-online analysis method based on 'angular streaking' [15, 29, 30]. In this scheme, illustrated in Figure 1, the total set of stochastic pulse shapes can be

sorted by an evaluation algorithm for suitable temporal structures. In recent experiments, angular streaking was already used to determine an overall regime of attosecond pulse durations for specific FEL operation modes, without using the varying single-shot X-ray pulse structure as a parameter for further physical analyses [16, 19, 20]. For a complete picture, the described intricate nature of SASE FEL machines requires shot-by-shot diagnostics to ensure an accurate understanding of the pulse-shape-based effects on the sample.

Here, we report on the generation and characterisation of isolated attosecond pulses of up to 200 GW peak power at 990 eV photon energy and a duration as low as ~700 ± 150 as at the SASE-based European XFEL. For the characterisation of the single-shot angular streaking data, we utilised a well-established iterative approach [15] as well as a recently developed machine-learning (ML) technique [31], which allows for similar reconstruction quality using less computation time and bearing the potential for online pulse characterisation. Moreover, we present time-delayed pump/probe sequences of double-peak attosecond pulses with various delays, as well as systematically varying pulse duration distributions for two different operation modes. Due to the high intensity of these XFEL pulses, ionic or excited states of matter can be created efficiently, and the emerging dynamics can be interrogated via the very same pulse with fully determined characteristics [32–37]. We show this capability by simultaneously measuring attosecond X-ray pulse shapes and the duration-dependent formation of double-core-hole states in gaseous neon. Thus, we combine attosecond single-shot photoelectron spectroscopy of extremely short-lived transient species with state-specific resonant X-ray excitation, paving the way to further time-resolved studies of more complex quantum systems, e.g. organic molecules, where coupled electronic and nuclear dynamics can be disentangled.

2 Intense Attosecond X-ray Pulses

In this experiment, we used isolated attosecond X-ray pulses (hν = 990 eV) with a peak power of up to 200 GW, characterised directly in time on a single-shot basis. In this dataset, approximately 20 % of the shots were found to be shorter than 1 fs and approx. 3 % below 750 as, with the shortest pulses in the order of 700 as (Figure 2). In this work, all durations are given in terms of the temporal distance between the first and last points where the temporal power profile reaches a value of half of the maximum (full width at half maximum / FWHM).

To generate attosecond SASE pulses at the European XFEL, we used a combination of increasing the FEL gain and reducing the length of the lasing window of the electron bunches in the accelerator. We achieved this with the chirp-dispersion method [38], using a non-standard approach for controlling the dispersion, with the additional benefit of increasing the peak current. The nonlinear electron bunch compression settings were later relaxed to a more conventional level to produce slightly longer pulses for comparison (FEL Setting B in Figure 2). A more detailed description of this innovative attosecond pulse generation mechanism can be found in the SI and will be also presented elsewhere (Serkez, S. et al., in preparation).
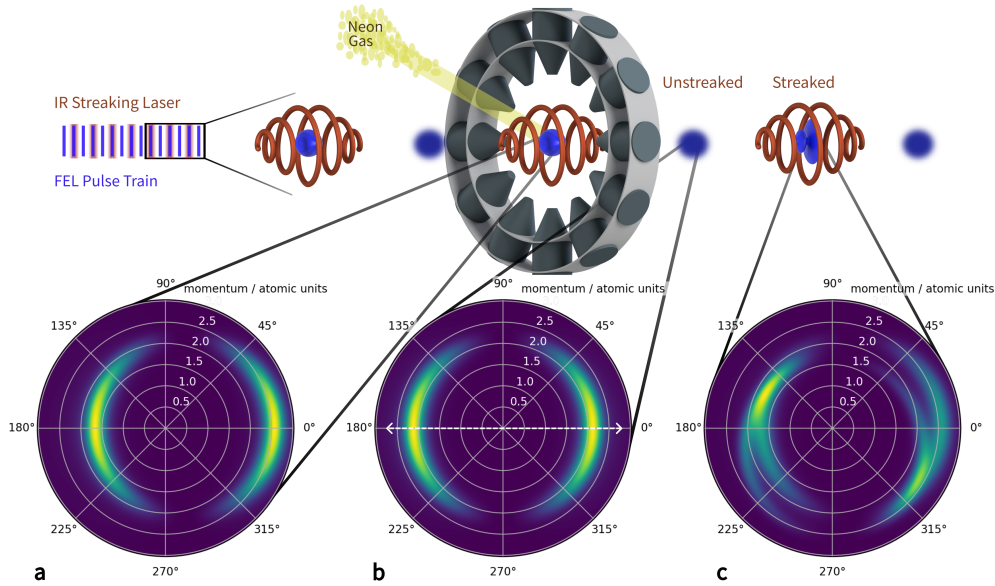
Fig. 1 Schematic overview of the angular streaking experiment. A train of XFEL pulses is overlapped with circularly polarised mid-infrared streaking laser pulses. The resulting phase-dependent electron energy shift is measured in a photoelectron spectrometer array. Three examples of simulated photoelectron spectra in the polarisation plane, **a)** a short (with respect to the optical cycle of the streaking laser) single pulse: shifted, here, to the right, **b)** an unstreaked shot (no shift), **c)** a double-peak pulse. The latter demonstrates best the capabilities of the method, as two rings appear in the angle-dependent photoelectron spectrum. With a suitable reconstruction algorithm, arbitrary XFEL pulse shapes can be reconstructed. The dashed white arrow indicates the X-ray polarisation, which imprints the angular distribution of photoelectrons through the transition's differential cross section.

Furthermore, in order to demonstrate the principal time-resolving capabilities, double-peak attosecond pulses, both at $h\nu = 990\,\text{eV}$, with individual single-peak powers close to 50 GW have been identified (Figure 3). Knowledge about the pulse structure allows sorting on peak power (as shown in section 4) as well as further analysis methods such as stochastic delay scans. As European XFEL is the first high repetition-rate XFEL in the world with >1000 shots per second, this 'post-sorting' yields the promise to get access to X-ray pump/X-ray probe methodology with highly intense pulses and attosecond time resolution. Figure 3 illustrates exemplary pulse structures in this regard. Together with the high photon energy from the XFEL, these pulses ultimately will allow for the required intensities that enable time-resolved insights into ultrafast *nonlinear* electronic processes.

3 SASE pulse characterisation

The measurement has been conducted at the SQS instrument of European XFEL, using the above-described highly compressed fresh-slice operation mode for generating X-ray pulses with durations entering the attosecond regime [12]. The temporal characteristics of the pulses can usually only be inferred indirectly in the SQS branch
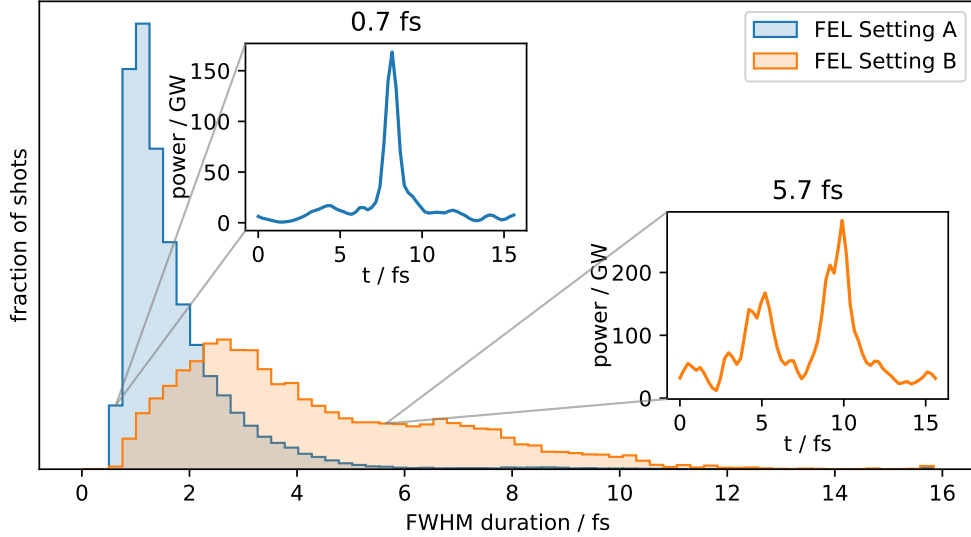
5

Fig. 2 Distribution of pulse FWHM duration for two evaluated machine operation modes, tuned for shortest possible pulses (Setting A) and longer pulses (Setting B). Insets: Example single pulse temporal shapes from the respective datasets.

of the beamline from destructive, i.e. photon-absorbing, measurements of the X-ray pulse spectra via a VLS-grating spectrometer [39] or indirect methods such as cross-correlation measurements [40, 41].

For fully characterizing the time–energy distribution of these pulses, we employ angular streaking, the only currently available direct and non-invasive method for characterizing the temporal and spectral X-ray structures of subsequent FEL pulses, i.e. the number of SASE peaks, the single-peak durations, and the SASE-pulse spectral chirp for each single shot (Figure 3). This knowledge can be used to find optimised FEL settings for targeted X-ray pulse characteristics, such as the shortest possible pulses, double-peak pulses with defined delay, or two-colour operation modes, as, for example, demonstrated in [42]. As the streaking technique in a low-density gas target is only negligibly influencing the X-rays with an absorption fraction on the sub-percent level, these same pulses can be used in a subsequent experiment, which can now capitalise on the fully determined X-ray characteristics via pulse tagging.

For this technique, a circularly polarised optical laser pulse is temporally and spatially overlapped with the X-ray FEL pulse in a region filled with neon gas at a partial pressure of approximately 10^{-7} hPa. The neon atoms are core-ionised by the XFEL pulse. The outgoing photoelectrons interact with the circularly polarised 4.75 μm mid-infrared (MIR) pulse, changing their momentum and leading to an energy and angular redistribution of the electrons depending on the electric field amplitude and phase of the streaking laser during the temporal window. The resulting angular and spectral distribution is detected by an array of 16 electron time-of-flight (eTOF)

6

spectrometers, positioned in a plane perpendicular to the joint propagation direction of the MIR laser beam and the FEL around the interaction point (Figure 1) [15].

In the present scheme, the retardation for all spectrometers can be set individually and was initially optimised to best resolve X-ray-ionised 1s photoelectrons. For neon and at an X-ray photon energy of 990 eV, these settings led to a photoelectron kinetic energy of $\sim$120 eV [43], allowing to robustly reconstruct the X-ray pulse shape with the applied angular-streaking technique. The maximum energy shift induced by the streaking laser is on the order of 15 eV. The spectral and temporal characteristics of individual pulses have been reconstructed using a post-experiment iterative retrieval code similar to the one published by Hartmann et al. [15].

This algorithm, described in more detail in subsection 3.1, is also adaptable to non-uniform configurations of eTOFs. For faster and more efficient online-feedback during future experiments, we established an ML-based evaluation pipeline (see subsection 3.2), implemented into the data read-out stream at the SQS instrument. Though the ML pipeline was running simultaneously during the measurement, providing single-shot X-ray pulse information at the full XFEL repetition rate, for the analysis presented in the following we relied on the iterative algorithm for a robust derivation of the pulse duration.

For the nonlinear dynamics measurement, we used the adaptability of our detector and the flexibility of the retrieval code to set the energy windows of 4 eTOF spectrometers to values outside the neon 1s electron acceptance window, deliberately dispensing with these eTOF spectrometers for the pulse characterisation. The acceptance energy of these 4 eTOF spectrometers was tuned instead to the expected energy of Auger electrons (recently also called Auger-Meitner electrons) emerging from so-called double core-hole (DCH) states [36] at much higher kinetic energies between 835 eV to 880 eV, while the other spectrometers remained at lower retardation voltages to ideally resolve the 1s photoelectrons for the X-ray pulse reconstruction of the corresponding shot. These combined single-shot measurements not only uncover the nonlinear dependency between X-ray pulse duration and DCH generation probability described in section 4, but further verify the attosecond X-ray pulse shape reconstruction due to its direct correlation with the DCH dynamics.

3.1 Iterative pulse reconstruction

To retrieve the temporal and spectral properties of the X-ray pulses via angular streaking, an algorithm called "PACMAN" [15] evaluates the photoelectron momentum distributions obtained by the eTOF spectrometers. In this algorithm, a simple semi-classical streaking simulation is run for a set of single-peak FEL pulses arranged on a time–energy grid, called basis. In every iteration, the best-fitting basis entry is subtracted incoherently from the data and an according intensity value is added to the resulting spectrogram at the point in time and photon energy corresponding to this entry. Repeating this process until the measurement is "consumed" results in a full spectrogram.

3.2 Machine-learning-based algorithm for online feedback

The main limitation of the iterative pulse reconstruction algorithm is the analysis speed, which currently does not allow for real-time feedback. The potential for using ML-based ultrafast diagnostic tools is vast. Li et al. [26] linked XFEL electron and photon beam properties to create an ML-based diagnostic tool; Alaa El-Din et al. [27] used ML to predict attosecond two-colour pulses; Brunner et al. [44] utilised ML to map from streaking traces to near-infrared pulses and electron wavepackets; Meng et al. [45] applied ML to learn the mapping from photon spectrograms to attosecond pulses using the all-optical method. In a recent article [31], we have shown that ML, particularly convolutional neural networks, in conjunction with angular streaking holds the potential for online XFEL pulse characterisation and, therefore, online diagnostics. We used these findings to implement an ML-based method that works during experimental campaigns and matches the quality of the iterative pulse reconstruction approach while only taking a fraction of its computation time.

We derived the desired pulse characteristics, such as the XFEL temporal pulse structure, from the detector images using the iterative reconstruction algorithm (cf. subsection 3.1) for generating labels from real-world experimental data, which we used for training the models in a supervised manner. A key challenge for model training is the limitation of labelled experimental data. We opted for a train–validation data split of 90%–10%, resulting in 65056 samples for training and 7232 samples for validation. Additionally, we held back 88 test samples to show the model's performance, which can later be used as prediction examples. Figure 4 shows three of the 88 test samples. By utilizing a dropout-based uncertainty technique [46], we can ensure validity of the model's prediction, which, in addition to further details on the ML pipeline, is detailed in the supplementary information. The ML predictions resemble the results of the iterative algorithm. The combination of angular streaking and ML evaluation, as shown here, is the first step towards closed-loop experimentation at XFELs [47].

4 Single-shot spectroscopy of transient states in neon

In the following, we use the attosecond temporal information about individual SASE pulses in a simultaneous measurement of an X-ray triggered process, leading to a better understanding of the ensuing nonlinear reaction dynamics. We sort individual X-ray shots according to their FWHM, revealing a clear peak-power dependence of the relaxation process in highly excited Ne ions. For this, we tune separate TOF detectors in the spectrometer setup to two different observation regions with respect to well-resolved electron energies: One set is kept at the previous energy at around 120 eV, given by direct photoionisation from the Ne 1s shell by a 990 eV X-ray pulse, which is used for the pulse reconstruction. The other, smaller set of TOF detectors is tuned to resolve higher electron energies, mainly between 760 eV and 920 eV, stemming from various Auger processes in the sample after illumination with intense X-ray pulses.

For a broad variety of relatively light elements with atomic numbers $Z < 30$, the Auger decay after K-shell ionization or excitation is the predominant relaxation mechanism, occurring typically within a few femtoseconds. Studying core-ionised systems
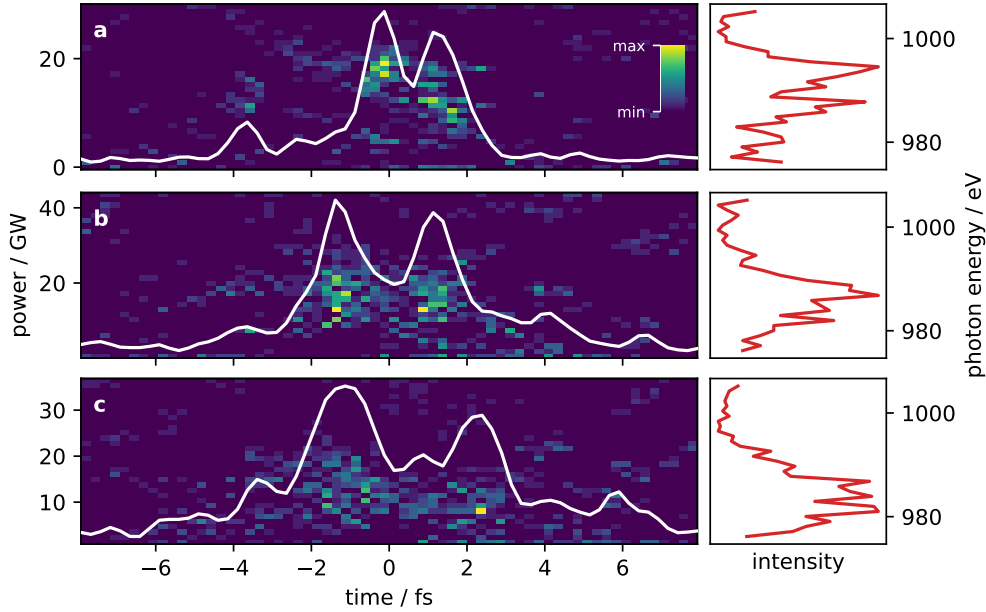
Fig. 3 a)–c) Three examples of reconstructed double-pulse structures. The colour-coded background represents the reconstructed spectrograms (full spectro-temporal information). Overlaid, the temporal shape of the FEL pulses is shown in white. The latter is normalised to the pulse energy to obtain an absolute power figure. The pulse energy is measured independently by the SQS X-ray gas monitor (XGMD). Right of the spectrograms, their projection onto the spectral axis is shown in red, representing an X-ray photon energy spectrum.

before the energy is transferred to the secondary Auger electron, promises insights into the localised non-equilibrium Coulombic environment of a transient system, preceding and thus governing any kind of X-ray-induced structural dynamics.

As shown in earlier studies of gaseous atomic neon, highly intense pulses of XFELs allow for sequential double photoionisation, where a core-ionised state is created by a first photon and this short-lived intermediate state is further core-ionised or core-excited by a second photon. In the photon picture, for such a process to occur, it is necessary that the absorption of the second photon precede the Auger decay of the single-core-hole state, which has a lifetime of 2.4 fs [48]. This second photon needs to overcome a significantly increased binding energy for the second K-shell electron in the transient neon $1s^{-1}$ system, which amounts to $\sim$1000 eV [36]. In this case, the core shell of the atom is left empty, termed a double-core hole. If the second K-shell electron is not promoted to the continuum but excited into one of the Rydberg states of the transient system, it becomes possible to spectroscopically map out the electronic structure of this very short-lived ionic system and observe rich information via the multitude of DCH Auger decay channels [49].

In Figure 5 **a)**, we present spectra of the resonant DCH decay in neon with high statistical robustness a) in a single FEL shot (blue solid line) in comparison to an average over 63329 shots (blue dotted line). For both cases in a) no streaking field was
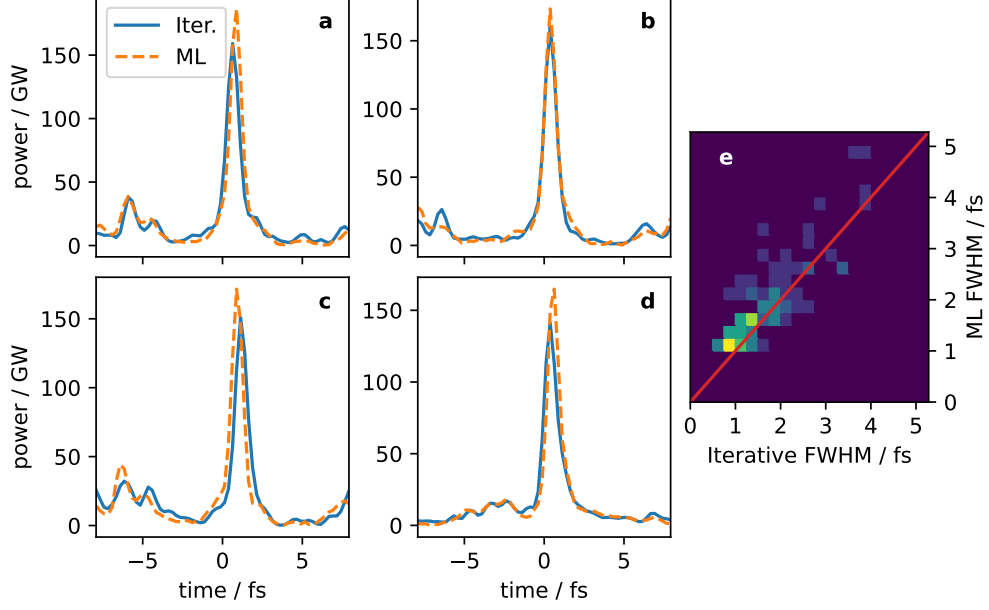
9

Fig. 4 a)–d) Ultrashort FEL pulse temporal structures derived from the iterative (solid blue line) and ML (dashed orange) reconstruction. The absolute power scale is calculated by normalizing the pulse shape to the total pulse energy. The latter is measured independently by the SQS X-ray gas monitor (XGMD). **e)** Correlation histogram of derived FWHM durations for both methods over all 88 evaluated shots, with red line indicating perfect agreement. The Pearson correlation coefficient for this sample is 0.83.

present. These unperturbed electron spectra were measured for every second X-ray shot during our experiment, allowing comparison with synchrotron spectra and photon energy calibration. The comparison clearly demonstrates that the highly intense attosecond pulses efficiently enable statistically robust spectroscopy of nonlinear processes for core-ionised neon atoms within single FEL shots. This allows for restrictive shot selection while retaining an adequate signal-to-noise ratio, despite challenging experimental conditions that prohibit long data acquisition times, which are generally not available at XFEL facilities.

In panel **b)** we show corresponding measurements on the streaked DCH signals, which were taken simultaneously with the X-ray pulse reconstruction spectra from the streaked 1s photolines for every other shot compared to **a)**. The average spectrum shown in **a)** is depicted in **b)** with the dotted blue line as well, for a better comparison of streaked spectra to the unstreaked spectrum. To preserve the energy resolution of the main DCH contributions, we have chosen the streaking phase in this representation such that the spectra are maximally shifted to higher energies under the given conditions, allowing to minimise the effect of spectral broadening of the Auger peaks by the streaking laser kick. The streaked spectra are depicted by coloured lines and indicate subsequently higher peak powers of the X-ray pulses, growing from yellow to black. The total FEL pulse energy is selected in a narrow window of $250\,\mu J \pm 10\,\mu J$,
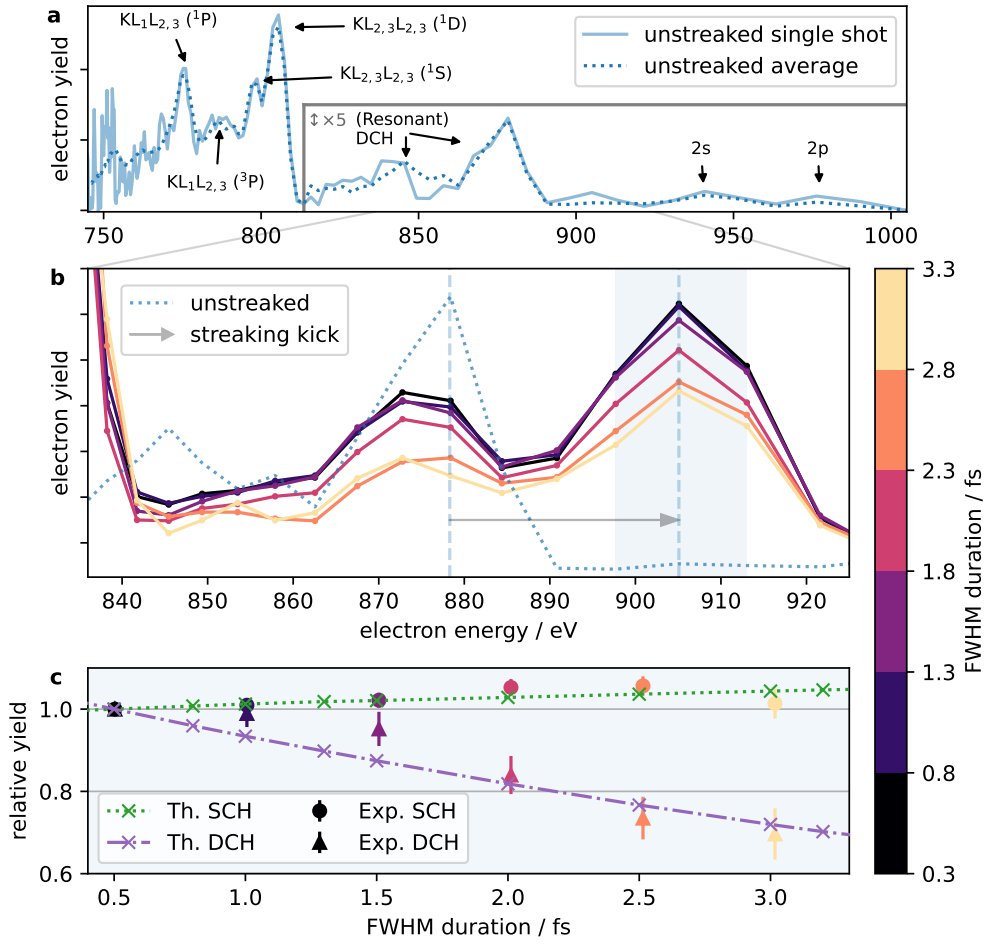
10

Fig. 5 a) Electron spectra of neon irradiated with intense 990 eV FEL pulses, with the infrared laser off ("unstreaked"), in single shot (solid line) and averaged over thousands of shots (dotted line). Single-core-hole Auger lines are visible in the energy range up to 804 eV, followed by resonant and non-resonant double-core-hole Auger peaks, measured with slightly coarser energy resolution. Valence photoelectrons are visible at the highest energies. **b)** Averaged electron spectra with the infrared laser on ("streaked"), filtered for a specific streaking laser phase and sorted by pulse duration. Phase and duration are determined from the pulse reconstruction using 8 other time-of-flight detectors tuned to 1s photoelectrons, instead of the Auger electrons shown here. Furthermore, only shots within a narrow pulse energy window of $250 \pm 10\,\mu\mathrm{J}$ are selected. The grey arrow indicates the energy shift induced by the infrared field, when compared to the spectrum without laser (also shown here as dotted line). **c)** The spectrum in **b)** is integrated over the light-blue shaded area to produce a relative yield curve as a function of pulse duration (triangles) for the double-core-hole peak. For comparison, a single-core-hole contribution is shown with circles. The single-core-hole yield is approximately constant, while, for a fixed number of photons, the double-core-hole yield drops off significantly for longer pulse durations. A theoretical model for both yields based on rate equations is shown as green dotted (SCH) and purple dash-dotted (DCH) lines.

11

keeping the total number of photons approximately constant. This demonstrates the clear peak power and thus pulse duration dependence of the nonlinear DCH signal increase [50].

Integrating the DCH peak signals within the blue shaded areas results in the signal yields plotted as triangular shapes in panel **c)**. Both curves are normalized to their respective first data points, to enable the comparison with the integrated single-core hole (SCH) yields from the "normal" Auger decay (circles) on the same scale. Several considerations need to be taken into account for the interpretation of the displayed FWHM dependence in Figure 5 **c)**. Under the given conditions, the total number of photons will predominantly determine the amount of SCH-Auger electrons, i.e. the single-photon-absorption processes scale linearly with the absolute intensity. Since the next step for creating a DCH requires a second photon in a direct sequence before the Auger relaxation can happen, it scales quadratically with the number of photons under the assumption that target depletion is negligible. For the data shown in Figure 5 **c)** we kept the pulse energy and thus the number of photons practically constant. However, by reducing the pulse duration, the *peak* power is increased, which leaves the amount of SCH unchanged, but still increases the DCH yield. This is true until the pulse duration becomes shorter than the Auger lifetime. At this point, the FWHM dependence for the DCH formation should vanish for the fluence of the given experimental conditions, since all DCH events stem from an excitation process that is faster than the core-hole lifetime. In panel **c)**, the DCH signals show the expected dependence on the FWHM of the reconstructed intensity profiles and thus on the peak power of single X-ray shots, while the SCH yields stay mostly flat over the whole FWHM range. This highlights the ability to employ attosecond-scale knowledge about individual SASE XFEL pulses to uncover otherwise hidden time-dependent nonlinear effects, based on the measurement of shot-to-shot X-ray pulse shape variations within a single FEL operation mode.

We compare our experimental findings with the results of a theoretical description of the DCH generation process based on a rate equation approach. The SCH and DCH Auger yields were simulated by solving a set of coupled rate equations using calculated atomic cross section and Auger decay lifetimes [51, 52].

Details about the employed theoretical methods and the rate equation calculations can be found in the SI. More sophisticated simulations based on full quantum mechanical descriptions reveal nonlinear dependencies on even higher ionisation states in neon. Further investigations of specific reaction pathways and their impact on the timescale of electron dynamics and on the lifetime of excited electronic states will be conducted in the future in order to answer such questions quantitatively.

5 Summary and Outlook

Enabled by the high intensity of the employed attosecond pulses at $990\,\text{eV}$, we thus have shown new paths to nonlinear spectroscopy of highly transient states of matter with X-rays. The state-specific exploration of electron dynamics via coherent attosecond X-ray pulses is a promising perspective towards exploring the physical origins of reaction processes together with the subsequent chemical evolution and ultimately a

system's functionality. Here, we have demonstrated the generation and measurement of isolated attosecond pulses of up to 200 GW peak power with durations of only about 700 as, opening up the potential for high-repetition rate XFELs to enable studies of nonlinear phenomena in transient media. While the technique presented here allows for studying details of electronic motion and redistribution, it can also readily map out their translation into nuclear dynamics. This method may be used in the future to directly follow electron rearrangement after excitation of specific elements in complex molecules, with the goal to sense and control the evolution of dynamical chemistry with atomic precision and to understand radiation damage mechanisms on a more fundamental level. Intriguing prospects of tracking electron migration in larger molecules such as peptides and amino acids and understanding the mechanisms of functionality-altering energy deposition and subsequent molecular restructuring are opened up. Combining the presented modes with the future possibilities of X-ray polarisation control at FELs will even allow studying the static and time-dependent asymmetric structures of such systems and their chiral dynamics.

References

[1] Paul, P. M. *et al.* Observation of a Train of Attosecond Pulses from High Harmonic Generation. *Science* **292**, 1689–1692 (2001).

[2] Hentschel, M. *et al.* Attosecond metrology. *Nature* **414**, 509–513 (2001).

[3] Uiberacker, M. *et al.* Attosecond real-time observation of electron tunnelling in atoms. *Nature* **446**, 627–632 (2007).

[4] Cavalieri, A. L. *et al.* Attosecond spectroscopy in condensed matter. *Nature* **449**, 1029–1032 (2007).

[5] Stockman, M. I., Kling, M. F., Kleineberg, U. & Krausz, F. Attosecond nanoplasmonic-field microscope. *Nature Photonics* **1**, 539–544 (2007).

[6] Lewenstein, M., Balcou, P., Ivanov, M. Y., L'Huillier, A. & Corkum, P. B. Theory of high-harmonic generation by low-frequency laser fields. *Physical Review A* **49**, 2117–2132 (1994).

[7] Shiner, A. D. *et al.* Wavelength Scaling of High Harmonic Generation Efficiency. *Physical Review Letters* **103**, 073902 (2009).

[8] Barletta, W. *et al.* Free electron lasers: Present status and future challenges. *Nuclear Instruments and Methods in Physics Research Section A: Accelerators, Spectrometers, Detectors and Associated Equipment* **618**, 69–96 (2010).

[9] Lutman, A. A. *et al.* Experimental Demonstration of Femtosecond Two-Color X-Ray Free-Electron Lasers. *Physical Review Letters* **110**, 134801 (2013).

[10] Emma, C. *et al.* Experimental demonstration of fresh bunch self-seeding in an X-ray free electron laser. *Applied Physics Letters* **110** (2017).

[11] Huang, S. *et al.* Generating Single-Spike Hard X-Ray Pulses with Nonlinear Bunch Compression in Free-Electron Lasers. *Physical Review Letters* **119**, 154801 (2017).

[12] Lutman, A. A. *et al.* Fresh-slice multicolour X-ray free-electron lasers. *Nature Photonics* **10**, 745–750 (2016).

[13] Emma, P. *et al.* Femtosecond and Subfemtosecond X-Ray Pulses from a Self-Amplified Spontaneous-Emission–Based Free-Electron Laser. *Physical Review Letters* **92**, 074801 (2004).

[14] Duris, J. *et al.* Tunable isolated attosecond X-ray pulses with gigawatt peak power from a free-electron laser. *Nature Photonics* **14**, 30–36 (2020).

[15] Hartmann, N. *et al.* Attosecond time–energy structure of X-ray free-electron laser pulses. *Nature Photonics* **12**, 215–220 (2018).

[16] Guo, Z. *et al.* Experimental demonstration of attosecond pump–probe spectroscopy with an x-ray free-electron laser. *Nature Photonics* (2024).

[17] Franz, P. *et al.* Terawatt-scale attosecond X-ray pulses from a cascaded superradiant free-electron laser. *Nature Photonics* (2024).

14

[18] Young, L. *et al.* Roadmap of ultrafast x-ray atomic and molecular physics. *Journal of Physics B: Atomic, Molecular and Optical Physics* **51**, 032003 (2018).

[19] Li, S. *et al.* Attosecond coherent electron motion in Auger-Meitner decay. *Science* **375**, 285–290 (2022).

[20] Li, S. *et al.* Attosecond-pump attosecond-probe x-ray spectroscopy of liquid water. *Science* **383**, 1118–1122 (2024).

[21] Thibault, P. *et al.* High-resolution scanning x-ray diffraction microscopy. *Science* **321**, 379–382 (2008).

[22] Ho, P. J. *et al.* The role of transient resonances for ultra-fast imaging of single sucrose nanoclusters. *Nature Communications* **11**, 167 (2020).

[23] Helml, W. *et al.* Ultrashort Free-Electron Laser X-ray Pulses. *Applied Sciences* **7**, 915 (2017).

[24] Milton, S. V. *et al.* Exponential gain and saturation of a self-amplified spontaneous emission free-electron laser. *Science (New York, N.Y.)* **292**, 2037–2041 (2001).

[25] Sanchez-Gonzalez, A. *et al.* Accurate prediction of X-ray pulse properties from a free-electron laser using machine learning. *Nature Communications* **8**, 15461 (2017).

[26] Li, K. *et al.* Prediction on X-ray output of free electron laser based on artificial neural networks. *Nature Communications 2023 14:1* **14**, 1–9 (2023).

[27] Alaa El-Din, K. K. *et al.* Efficient prediction of attosecond two-colour pulses from an X-ray free-electron laser with machine learning. *Scientific Reports 2024 14:1* **14**, 1–10 (2024).

[28] Decking, W. *et al.* A MHz-repetition-rate hard X-ray free-electron laser driven by a superconducting linear accelerator. *Nature Photonics* **14**, 391–397 (2020).

[29] Li, S. *et al.* Characterizing isolated attosecond pulses with angular streaking. *Optics Express* **26**, 4531 (2018).

[30] Heider, R. *et al.* Megahertz-compatible angular streaking with few-femtosecond resolution at x-ray free-electron lasers. *Physical Review A* **100**, 053420 (2019).

[31] Dingel, K. *et al.* Artificial intelligence for online characterization of ultrashort X-ray free-electron laser pulses. *Scientific Reports* **12**, 17809 (2022).

[32] Sorokin, A. A. *et al.* Photoelectric Effect at Ultrahigh Intensities. *Physical Review Letters* **99**, 213002 (2007).

[33] Young, L. *et al.* Femtosecond electronic response of atoms to ultra-intense X-rays. *Nature* **466**, 56–61 (2010).

[34] Rudek, B. *et al.* Ultra-efficient ionization of heavy atoms by intense X-ray free-electron laser pulses. *Nature Photonics* **6**, 858–865 (2012).

[35] Rudenko, A. *et al.* Femtosecond response of polyatomic molecules to ultra-intense hard X-rays. *Nature* **546**, 129–132 (2017).

[36] Mazza, T. *et al.* Mapping Resonance Structures in Transient Core-Ionized Atoms. *Physical Review X* **10**, 041056 (2020).

[37] Boll, R. *et al.* X-ray multiphoton-induced Coulomb explosion images complex single molecules. *Nature Physics* **18**, 423–428 (2022).

[38] Guetg, M. W., Lutman, A. A., Ding, Y., Maxwell, T. J. & Huang, Z. Dispersion-Based Fresh-Slice Scheme for Free-Electron Lasers. *Physical Review Letters* **120**, 264802 (2018).

[39] Gerasimova, N. *et al.* The soft X-ray monochromator at the SASE3 beamline of the European XFEL: from design to operation. *Journal of Synchrotron Radiation* **29**, 1299–1308 (2022).

[40] Rivas, D. E. *et al.* High-temporal-resolution X-ray spectroscopy with free-electron and optical lasers. *Optica* **9**, 429–430 (2022).

[41] Grychtol, P. *et al.* Timing and X-ray pulse characterization at the Small Quantum Systems instrument of the European X-ray Free Electron Laser. *Optics Express* **29**, 37429–37442 (2021).

[42] Li, S. *et al.* "Beam à la carte": laser heater shaping for attosecond pulses in a multiplexed x-ray free-electron laser (2024). URL http://arxiv.org/abs/2404.02299.

[43] Schmidt, V. *Electron Spectrometry of Atoms using Synchrotron Radiation* Cambridge Monographs on Atomic, Molecular and Chemical Physics (Cambridge University Press, Cambridge, 1997).

[44] Brunner, C. *et al.* Deep learning in attosecond metrology. *Optics Express, Vol. 30, Issue 9, pp. 15669-15684* **30**, 15669–15684 (2022).

[45] Meng, L. *et al.* Deep learning for isolated attosecond pulse reconstruction with the all-optical method. *JOSA B, Vol. 40, Issue 10, pp. 2536-2545* **40**, 2536–2545 (2023).

[46] Gal, Y. & Ghahramani, Z. Balcan, M. F. & Weinberger, K. Q. (eds) *Dropout as a bayesian approximation: Representing model uncertainty in deep learning.* (eds Balcan, M. F. & Weinberger, K. Q.) *Proceedings of The 33rd International*

Conference on Machine Learning, Vol. 48 of *Proceedings of Machine Learning Research*, 1050–1059 (PMLR, 2016). URL https://proceedings.mlr.press/v48/gal16.html.

[47] Dingel, K. in *Actively controlling and redesigning experiments using the application case of free-electron laser pulse characterization* (eds Tomforde, S. & Krupitzer, C.) *Organic Computing – Doctoral Dissertation Colloquium 2021* 86–98 (kassel university press, 2022).

[48] Haynes, D. C. *et al.* Clocking Auger electrons. *Nature Physics* 1–7 (2021).

[49] Mazza, T. *et al.* Resonant Raman Auger spectroscopy on transient core-excited Ne ions. *Journal of Physics B: Atomic, Molecular and Optical Physics* (2024).

[50] Inhester, L., Hanasaki, K., Hao, Y., Son, S.-K. & Santra, R. X-ray multiphoton ionization dynamics of a water molecule irradiated by an x-ray free-electron laser pulse. *Phys. Rev. A* **94**, 023422 (2016).

[51] Bhalla, C. P., Folland, N. O. & Hein, M. A. Theoretical K-Shell Auger Rates, Transition Energies, and Fluorescence Yields for Multiply Ionized Neon. *Phys. Rev. A* **8**, 649–657 (1973).

[52] Gryzlova, E. V., Kiselev, M. D., Popova, M. M. & Grum-Grzhimailo, A. N. Evolution of the ionic polarization in multiple sequential ionization: General equations and an illustrative example. *Phys. Rev. A* **107**, 013111 (2023).